PRIFYSGOL
**BANGOR**
UNIVERSITY

**Three-dimensional modelling of turbine wake interactions at a tidal stream energy site**

Michelet, Nicolas; Guillou, Nicolas; Chapalain, Georges; Thiebot, Jerome; Guillou, Sylvain; Goward Brown, Alice; Neill, Simon

**Applied Ocean Research**

Cyswllt i'r cyhoeddiad / Link to publication

# Three-dimensional modelling of turbine wake interactions at a tidal stream energy site

5    **Michelet N.[1], Guillou N.[1,*], Chapalain G.[1], Thiébot J.[2], Guillou S.[2], Goward Brown A.J.[3], Neill S.P.[3]**

1- Cerema/DtecEMF/ER/Laboratoire de Génie Côtier et Environnement (LGCE), 155 rue Pierre Bouguer, Technopôle Brest-Iroise, BP 5, 29280 Plouzané, France

10   2- Normandie Univ., UNICAEN, LUSAC, EA4253, Site de Cherbourg, 60 rue Max-Pol Fouchet, CS 20082, 50130 Cherbourg-en-Cotentin, France

3- School of Ocean Sciences, Bangor University, Menai Bridge, United-Kingdom

* nicolas.guillou@cerema.fr, corresponding author

15

**Abstract:** One of the biggest uncertainties in tidal stream energy resource assessment is how tidal energy conversion, particularly at large scale, will interact with the resource. As few arrays are currently operational, data collected from these developments tends to be commercially sensitive. Therefore, array interaction with the

20   resource is generally assessed using numerical models. A fully three-dimensional numerical approach based on Actuator Disk theory was implemented into the Regional Ocean Modelling System (ROMS) to simulate the energy extraction by tidal stream turbines. Emphasis was placed on wake interactions and cumulative effects of individual devices on energy extraction at array scale. This model was applied at the tidal stream energy site of the Fromveur Strait (western Brittany, France) considering an array of horizontal-axis turbines of 10-m diameter,

25   matching the device technology currently operating in the Strait. Two tidal energy metrics were considered to describe asymmetries in tidal current magnitude and direction. The area with reduced asymmetry in current magnitude was selected to implement the turbine array. A nested grid technique was adopted to cascade processes from the regional scale to the high-resolution local farm domain. The computation was conducted over the inner-nested array domain covering the tidal farm with horizontal and vertical resolutions of 1 m, matching

30   the 1/10th turbine diameter (D) recommended to resolve velocity and turbulence intensity along device wakes. The array layout initially followed recommended staggered configurations with longitudinal and lateral spacings of 10D and 5D, respectively. However, during mean spring tidal conditions, the misalignment of peak flood currents induced significant wake interactions that reduced the array output by about 15% in comparison to peak ebb. These interactions were investigated to adapt array layouts, minimise wake interactions, and optimise the

35   energy conversion. By reducing the lateral spacing between devices to 3D (measured centre to centre rather than tip to tip), the flood ebb asymmetry in energy extraction was lowered from 15% to 2%.

**Keywords :** Array layout; Tidal asymmetry; Misalignment; Actuator Disk; ROMS; Fromveur Strait.

40

# 1. Introduction

The development of more sustainable forms of energy conversion appears, at the present time, as part of the solution to meet the global growing need for electricity demand, while reducing the exploitation of fossil fuel reserves and limiting the impacts of climate change and global warming. A growing attention is thus being paid to low carbon renewable resources including solar, wind and ocean energy. Among the different types of marine renewable resources, the kinetic energy of tidal currents offers the major advantage of being highly predictable with reduced visual impacts, promoting their acceptance for coastal communities. Over the last decade, the exploitation of this resource has led to considerable technological developments with a series of prototypes tested in real sea conditions [1,2,3]. However, refined assessments of the interactions between tidal energy converters and the marine environment are required to guarantee successful deployment of multiple devices within stream energy sites.

The most common way to characterise the complex hydrodynamics of tidal stream energy sites relies on high-resolution numerical modelling validated by in-situ observations. Regional simulations were conducted to assess the available tidal kinetic energy resource in the most promising locations for the deployment of tidal turbines including the north-western European shelf seas [4,5,6,7], the coasts of USA and Canada [8,9], the south Japan sea [10], and the Brazilian shelf [11]. These numerical assessments provided further insights about the spatial and temporal variabilities of the available resource. However, accurate representations of the interactions between devices' wakes and the ambient flow field are required to evaluate the technically exploitable energy and the hydrodynamic effects induced by tidal stream energy extraction.

The interactions between tidal stream turbines and the marine environment were initially investigated with two-dimensional depth-averaged models that represented the tidal farm as an area with enhanced bed friction parameterised by averaging the turbines drag forces [12,13]. At the early stages of a tidal-farm project, this equivalent drag approach provides, with reduced computational cost, an assessment of the large-scale effects of tidal-stream energy extraction. However, the processes at the scale of the array were coarsely represented, especially wake interactions that are likely to result in uncertainties in the assessment of the hydrodynamic impact of the farm and its power output.

More refined three-dimensional approaches were considered to represent the effects of individual turbines on the tidal flow by relying on advanced Computational Fluid Dynamics (CFD) techniques. These effects were simulated using the Actuator Line (AL) or the Blade Element Momentum Theory (BEMT) methods. Those methods are based on distributing the external loading (lift and drag) along the blade's axial direction [14,15,16,17]. Rotating turbines can also be represented using fully-meshed turbines (where the structure is physically represented in the model) [18,19,20]. Whereas those advanced CFD methods provide accurate representation of turbines' effects on the tidal flow, the numerical applications require refined spatial resolution (<< 1 m) and are thus generally restricted to the representation of a single device, setting aside a description of multiple turbine wake interactions within the array.

In contrast to these advanced techniques the Actuator Disk (AD) method appears as a simple and efficient approach, compatible with regional tidal circulation modelling, to simulate interactions of horizontal-axis turbines within a given array [21,22,23]. In this method, the turbine is represented as a porous disk, and forces are integrated equivalent to the resistance of this disk as a sink term in the momentum equations of the tidal circulation model. However, the force is distributed over the area swept by the turbine blades, which also requires refined spatial resolutions, leading to increased computational cost. Nevertheless, as demonstrated by Liu et al. [24], this simple approach was able to provide results comparable with more advanced modelling techniques including the rotational effects of turbine blades such as the Moving Frame Reference or the Sliding Mesh approaches. In the same way, Shives and Crawford [25] proposed a tuning procedure of the AD method based on the fitting of the thrust and power coefficients to obtain reliable predictions with ANSYS CFX of turbine wakes against experimental results reported by Mycek et al. [26,27], in a large variety and ambient turbulence intensity and incoming velocities. However, with few exceptions [e.g., 23,28], the application of the AD method was restricted to small spatial and temporal domains using idealised bathymetry and forcing conditions [21,22,29,24]. Among these numerical studies, Nguyen et al. [30] compared the impacts of four turbulence models on wake predictions behind an AD by relying on the experimental observations conducted by Harrison et al. [22] exhibiting the performance of the k-ε turbulence closure.

Nevertheless, this method poses a promising improvement to the enhanced drag approach, for determining the interactions of a turbine array with the hydrodynamic conditions. Significant differences are, in particular, expected in tidal stream energy sites characterised by asymmetries in tidal current magnitude and direction between the flood and ebb phases of the

3

tidal cycle [31,32]. In the Orkney archipelago (Scotland, the United-Kingdom), Neill et al. [31] reported that a 30% asymmetry in tidal current velocity may result in a 100% asymmetry in power density. More recently, in the "Raz de Sein" (western Brittany, France), Guillou and Chapalain [32] showed that a yearly-averaged misalignment of 32° between ebb and flood current peaks may lead to a 12% reduction of the monthly-averaged extractable energy. However, these numerical studies were established by relying on device power curves, setting aside the effects of turbines on the ambient flow field. The implementation of the AD method at a real tidal stream energy site is thus a first step towards developing a better understanding of the effect of tidal current asymmetry on turbine wake interactions within an array.

The present study investigates wake interactions at the scale of an array at a real tidal stream energy site by applying a fully three-dimensional approach based on the AD method. The site of application is the Fromveur Strait, off western Brittany, which separates the island of Ushant from the Molène archipelago (Fig. 1). With mean spring tidal currents exceeding 4 m s$^{-1}$, this area was identified by the French Government as one of the primary locations for the implementation of tidal stream turbines in French coastal waters. A restricted area of 4 km$^2$ was thus identified within the Fromveur Strait for the development of tidal stream projects. A series of numerical investigations were conducted at this site to refine the quantification of the available tidal kinetic energy [7, 13, 33, 34]. High-resolution depth-averaged circulation models were also implemented to evaluate the far-field effects induced by tidal stream energy extraction (represented as an equivalent drag) on the hydrodynamics and water-mass transport [13, 35, 36]. In contrast to these previous studies, the present contribution simulated the flow within the array and analysed its performance in terms of power output to adapt array layouts and maximise power output. To match the Sabella D10 technology turbines currently operating in the Strait, the modelled array integrated horizontal-axis turbines with a diameter of 10m. The purpose of the tidal array is to meet between 15 and 20% of the electricity demand of the island of Ushant, currently provided by a fossil fuel power station. With the view of fulfilling a significant part of the energy need of the island with tidal stream energy, an array of eight devices was thus considered with two staggered configurations varying in the lateral and longitudinal spacings between turbines. The AD method was furthermore included with constant thrust coefficient in order to simplify the analysis of numerical predictions neglecting further information regarding the turbine's technology such as its power curve or structural drag.

Numerical simulations were based on the Regional Ocean Modelling System (ROMS, [37]) (Section 2.1) modified to include the AD sub-model (Section 2.2). The model was 140 implemented in a series of embedded computational domains ranging from the scale of western Brittany to the array scale (Section 2.3). Predictions were assessed against available in situ measurements and an established database of tidal currents within the region of interest (Section 3.1). The detailed hydrodynamic characteristics of the Fromveur Strait were examined, focusing on the asymmetries of tidal currents in both magnitude and direction 145 during mean spring tidal conditions (Section 3.2). Two different turbine array configurations were compared, both centred on an area characterised by symmetry in current magnitude. Particular emphasis was placed on device wake interactions and power output (Sections 3.3 and 3.4).
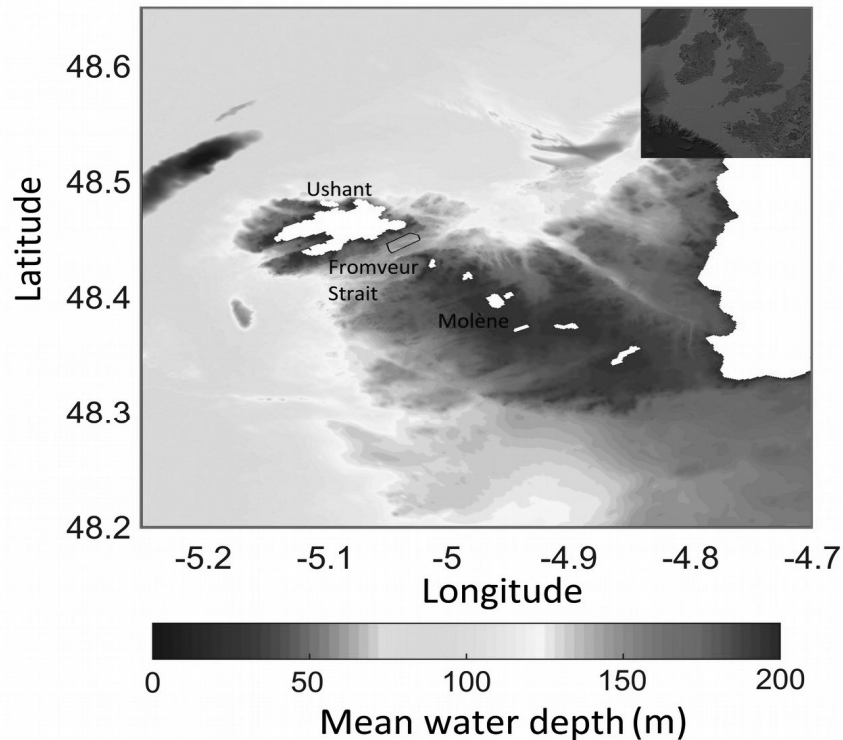


Figure 1 - Bathymetry of the Ushant-Molène archipelago. The black outline in the Fromveur Strait delimits the area of interest identified by the French Government for the implementation of an array of turbines. Water depth (in metres) is relative to mean sea level.

5

# 2. Method

## 2.1. ROMS model description

ROMS is a three-dimensional, free-surface numerical model that solves finite-difference approximations of the Reynolds-Averaged Navier Stokes (RANS) equations using the hydrostatic and Boussinesq approximations. The flow is assumed to be turbulent over a rough bottom, characterised by the roughness parameter $z_0$ defined as the height above the sea bed at which the fluid velocity is zero. The numerical computation is performed with curvilinear coordinates in the horizontal and terrain-following $\sigma$ coordinates in the vertical. The horizontal eddy viscosity is parameterised with the Smagorinsky formulation [38]. The vertical eddy viscosity is expressed as $\upsilon_T = 0.096\, k^2/\varepsilon$, where $k$ is the turbulent kinetic energy and $\varepsilon$ is its dissipation rate. These turbulent parameters are obtained by solving a pair of transport equations, known as the $k$-$\varepsilon$ model and derived from the Generic Length Scale (GLS) formulation [39]. The momentum and turbulent equations are subjected to boundary conditions at the sea bed and the sea-surface. The bottom conditions derive from the law-of-the-wall, while surface conditions consider zero gradients of the horizontal velocity. The set of equations is finally resolved using the mode-splitting technique that separates the barotropic and baroclinic modes [40]. The algorithms that comprise ROMS computational non-linear kernel are described in Shchepetkin and McWilliams [37] and further details are available in Haidvogel et al. [41].

## 2.2. Tidal turbine representation

Actuator Disk theory is based on the application of a retarding force $F_t$ in the momentum equation to represent the stream energy extraction induced by a porous disk whose resistance is assumed equivalent to the thrust of the turbine (Fig. 2). This force, which is applied over the surface swept by the blades, results from a pressure discontinuity over the disk, and is defined, from the Bernouilli's equation, as:

$$F_t = A\,\Delta p = \frac{1}{2}\rho A \left( u_\infty^2 - u_w^2 \right) \tag{1}$$

where $\Delta p$ is the pressure drop between the upstream and downstream sides of the disk, $A$ is the disk surface, $\rho$ is the fluid density, and $u_\infty$ and $u_w$ are the upstream and downstream velocities, respectively. This retarding force can also be expressed, from the conservation of mass along the stream-tube control volume, as

$$F_t = \rho A u_d (u_\infty - u_w) \qquad (2)$$

190 where $u_d$ is the local velocity within the disk. This velocity is thus determined, from equations 1 and 2, as

$$u_d = \frac{1}{2}(u_\infty + u_w) . \qquad (3)$$

Combining equations (1) and (3), the retarding force is finally expressed, from the local velocity $u_d$, as

$$F_t = \frac{1}{2}\rho A C_t \left(\frac{u_d}{1-a}\right)^2 . \qquad (4)$$

where $a=(u_\infty - u_d)/u_\infty$ is the axial flow induction factor and $C_t = 4a(1-a)$ is the thrust coefficient.

195 According to Betz [42], the maximum extractable power is obtained for an induction factor of $a=1/3$, which corresponds to a thrust coefficient of $C_t=0.9$. These values were adopted in the present study.

The thrust force is applied along the direction normal to the surface covered by the turbine blades. Considering that the x-axis of the computational grid is orientated along this direction,

200 the thrust force is applied as a sink term in the associated momentum equation. This sink term is defined as S= -$F_t$/(Ae) where $e$ is the disk thickness considered equal to the grid resolution $\Delta x$ in the (Ox) direction. AD theory does not consider the motion of the turbine blades, and so swirl effects and tip vortices shed by the blades are omitted. However, those effects are known to dissipate rapidly and to become insignificant in the far-wake (at a distance >7D from the

205 turbines blades) where AD provided reliable predictions of velocity deficit and turbulent intensity [22]. AD theory is therefore considered here as a suitable approach to represent, in a numerical model, the turbine wake interactions within an array [43,44].

Finally, the power captured by a single device is determined as

$$P_{ext} = \frac{1}{N}\sum_{i=1}^{N}\frac{1}{2}\rho A C_p \left(\frac{u_{d,i}}{1-a}\right)^3 \qquad (5)$$

210 where $N$ is the number of computational nodes within the disk area, $u_{d,i}$ is the local velocity at the computational node $i$ within the disk area, and $C_p$ is the electrical power coefficient, set here to 0.35 according to Myers and Bahaj [45].
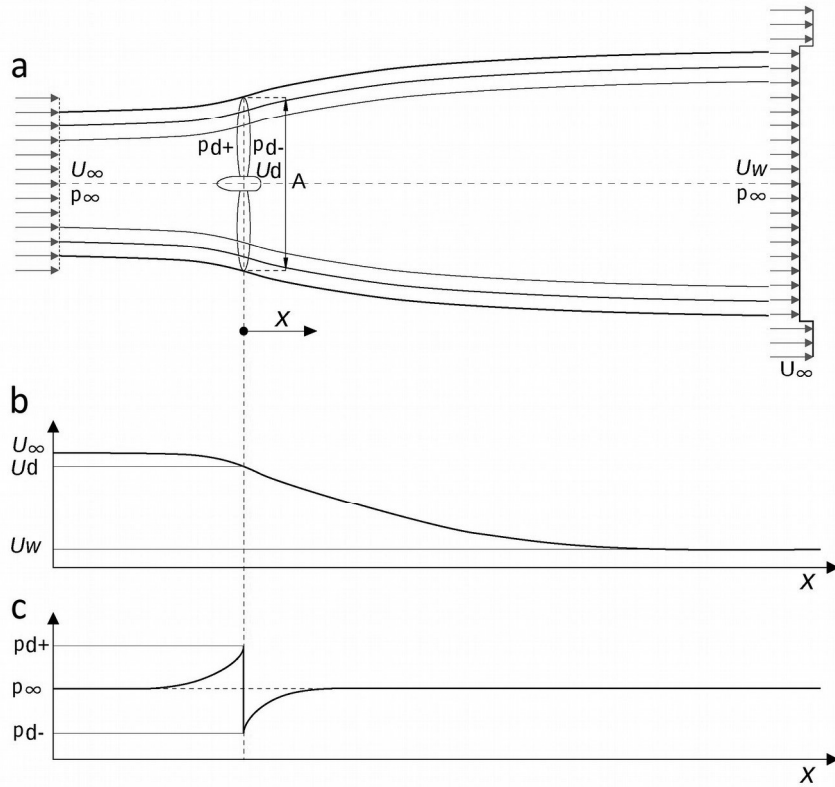
7

Figure 2 - (a) Schematic representation of the AD method, and variations of (b) current magnitude and (c) pressure along the stream tube [after 46].

215

## 2.3. Model setup

Preliminary regional simulations with computational grids aligned along the longitude and the latitude were performed to determine the prevailing current direction in the Fromveur Strait, and initial orientation of the turbines. Those predictions exhibited the rectilinear 220 characteristics of tidal currents in the tidal energy site, with a north-eastern orientation of 20° with respect to the longitude. The horizontal computational grids were thus rotated by 20° so that the retarding force was integrated as a sink term in the momentum equations along the (Ox) direction (Fig. 3). Further simulations were conducted to determine the horizontal and vertical spatial resolutions of the computational grid at the scale of the turbines array. 225 Following the investigations of Roc et al. [47], Nguyen et al. [30] and Thiébot et al. [44], the modified version of ROMS with the AD model was first assessed against the flume experiment of Myers and Bahaj [48], that consisted of measuring the velocity and turbulent intensity profiles in the wake of a non-rotating porous disk with a diameter of 0.1 m subjected to a steady-state inflow of 0.33 m s$^{-1}$ in a water depth of 0.3 m. A minimum spatial resolution

230 of 1 m was required in the three directions (Ox), (Oy) and (Oz) to approach measurements at a distance of seven rotor diameters from the disk. Sensitivity tests conducted at the ocean scale matching the geometric and hydrodynamic conditions of the Fromveur Strait confirmed this minimum spatial resolution of $1/10^{th}$ the turbine diameter.

Considering turbines with a diameter of 10 m, the minimum spatial resolution of 1 m
235 within the array was achieved by application of three-embedded computational domains G1, G2, and G3 orientated with an angle of 20° with respect to the longitude (Fig. 3). The outer domain (G1) covered the Sea of Iroise and extended from 6°W to 3.5°W in longitude, and from 47.3°N to 48.9°N in latitude with a grid size of 500 m and 25 vertical $\sigma$ layers. The intermediate domain (G2) covered the Ushant-Molène archipelago and extended from 5.3°W
240 to 4.6°W, and from 48.1°N to 48.6°N with a grid size of 100 m and 25 vertical $\sigma$ layers. Finally, the inner-nested array domain (G3) was located within the area identified by the French Government for the development of tidal array projects (Fig. 3b). This domain was centred on an area characterised by equivalent magnitude of tidal currents at the peak flood and ebb (Section 3.2). Indeed, as shown by Neill et al. [31], considering the asymmetry in
245 tidal current magnitude and focusing on a location with minimum asymmetry was important to reduce the variability of power output over the tidal cycle. Further, the horizontal grid dimensions of domain G3 were sufficiently large (1000 m x 200 m) to avoid boundary effects, since the nesting process was one-way. In the longitudinal direction, the boundaries were placed at a distance of 40 rotor diameters (40D) from the array so that complete flow recovery
250 was achieved before reaching the grid boundary [30]. The horizontal spatial resolution was set to 1 m in domain G3 and 50 vertical $\sigma$ layers were considered, the mean water depth being 50 m in the Fromveur Strait.
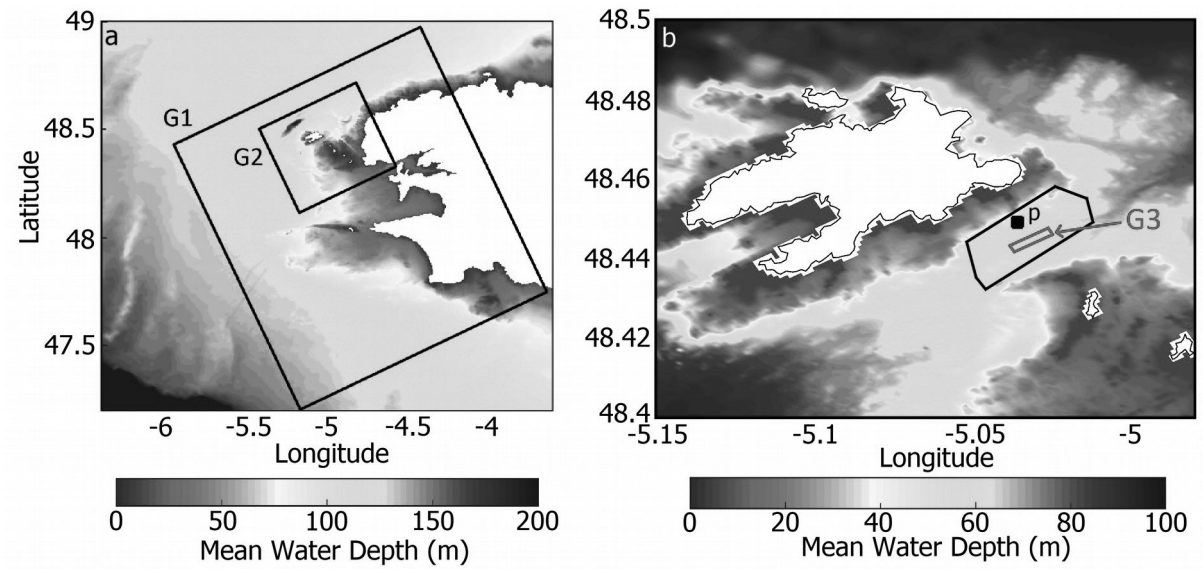
Figure 3 - (a) Boundaries of the outer (G1) and intermediate (G2) domains. (b) Magnified view of the Fromveur Strait with (black line) the area of interest for the implementation of tidal stream turbines and (red line) the inner-nested array grid (G3). Point p shows the location of the available ADCP mooring within the Fromveur Strait. Colour scale shows the spatial distribution of mean water depth, with respect to mean sea level.

In the innermost nested domain, G3, two arrays of eight turbines were considered. These turbines were numbered T1 to T8 and arranged in three rows, numbered from R1 to R3 and 255 comprising 3, 2 and 3 devices, respectively (Fig. 4). The first configuration C1 was defined following a staggered layout recommended by Bai et al. [21]. This layout is classically employed [44,49,50] as it should limit wake interactions when current direction is aligned with the turbine axes. It was thus defined with a longitudinal spacing of 10D and a lateral spacing of 5D (centre to centre) (Fig. 4). The second configuration C2 was defined to be 260 adapted to the hydrodynamic conditions within the Fromveur Strait in order to maximise power output. In this configuration the lateral spacing was reduced to 3D (Fig. 4). These configurations were consistent with the results obtained by Funke et al. [51] for optimising the design of tidal stream turbine farms, focusing on structures aligned perpendicular to the flow and concentrated around in local areas such as the region with equivalent magnitude of tidal 265 currents at the peak flood and ebb.
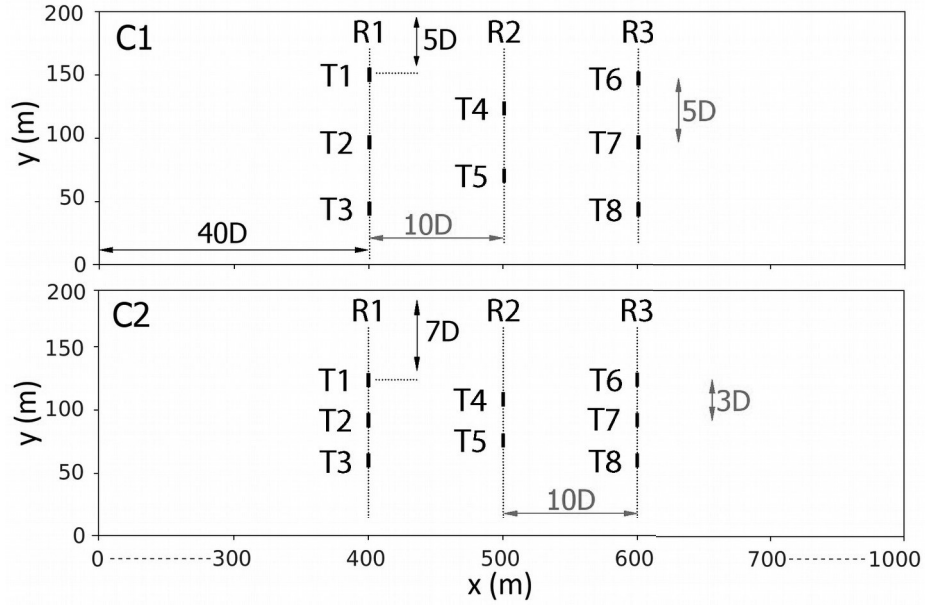
Figure 4 - Plan view of array configurations C1 and C2 with the distance from the domain boundaries.

The bathymetry was interpolated from a range of databases including (i) the regional database of Loubrieu et al. [52] with a spatial resolution of 1 km and (ii) the high-resolution database that covers the Ushant-Molène archipelago with a maximum spatial resolution of 5 m collected during the Litto3D project [53]. The bottom roughness parameter $z_0$ was defined at each computational node according to the distribution of sea bed sediment types determined from the map of Hamdi et al. [54]. Bottom roughness values adopted by Guillou and Thiébot [13] were implemented for the parametrisation of $z_0$. The model was forced by 13 harmonic tidal components ($M_2$, $S_2$, $N_2$, $K_2$, $K_1$, $O_1$, $P_1$, $Q_1$, $M_f$, $M_m$, $M_4$, $M_{N4}$, $M_{S4}$) using the TPXO7.2 database covering the region of interest at a spatial resolution of 0.25° [55]. Wind and wave contributions were neglected, and it should be noted that these meteorological conditions may influence the available tidal kinetic energy within the Fromveur Strait during storm conditions [33]. Coastal lateral boundaries were considered as impregnable walls using a free-slip condition. On the outer domain (G1), a Flather [56] condition was applied on the depth-averaged velocity components normal to the boundary. A Flather condition was also retained for the depth-averaged tangential components along the southern and northern boundaries, while a Chapman [57] condition was considered for the tangential components along the eastern and western boundaries. Three-dimensional variables were implemented using a radiation condition [58]. In the intermediate domain (G2), a nesting formulation from predictions established in G1 was applied to all variables. On the inner-nested domain that included the tidal array (G3), the lateral boundaries were driven by the results output from G2.

Accordingly, the Flather [56] formulation was applied on depth-averaged velocity components to ensure the propagation of the flow and a Dirichlet condition was applied on the other variables to force the vertical profiles of momentum and turbulent variables, and the variation of the free surface.

The numerical results were evaluated with statistical parameters that included the index of agreement *RE* described by Willmot [59] and the Mean Average Error $MAE = \frac{1}{n}\sum_{i=1}^{n}|sim_i - obs_i|$ where $n$ is the number of data points in the discretised series considered, and ($sim_i$) and ($obs_i$) (with i ∈ [1,$n$]) are the simulated and observed data, respectively. The asymmetry in tidal current magnitude between the ebb and flood phases was estimated, during mean spring tidal conditions, by relying on the tidal energy resource metrics considered by Guillou and Chapalain [32], and Guillou et al. [7] in western Brittany and the western English Channel, and defined as

$$A_s = 1 - \left( \frac{u_{peak,1}}{u_{peak,2}} \right) \tag{6}$$

where $u_{peak,2}$ is the maximum module of the peak velocity between flood and ebb, and $u_{peak,1}$ is the minimum peak velocity during the opposite phase of the tidal cycle. This parameter varies between zero and one. High values of $A_s$ account for significant tidal current asymmetry, while low values indicate more symmetrical currents. Following Lewis et al. [60] and Guillou et al. [7], the asymmetry in tidal current direction was also evaluated as

$$\beta_s = \arccos \left( \frac{-\overrightarrow{u_{peak,1}}\,\overrightarrow{u_{peak,2}}}{\|u_{peak,1}\|\|u_{peak,2}\|} \right). \tag{7}$$

High values of $\beta_s$ indicate strong tidal current misalignment, whereas low values indicate a reduced asymmetry in current direction.

Predictions from the inner-nested domain G3 were projected over a horizontal plane orthogonal grid at a reference elevation of 10 m above the bottom of a point located at the centre of the domain G3 (Fig. 5). This reference elevation corresponds to the height of the centre of a turbine with a diameter of 10 m, including a sea bed clearance of 5 m. This grid that disregards the seabed variation enables us to follow the spatial evolution of turbines

wakes with respect to a horizontal reference plane. This horizontal reference plane may thus be located below or above the different turbines centres.
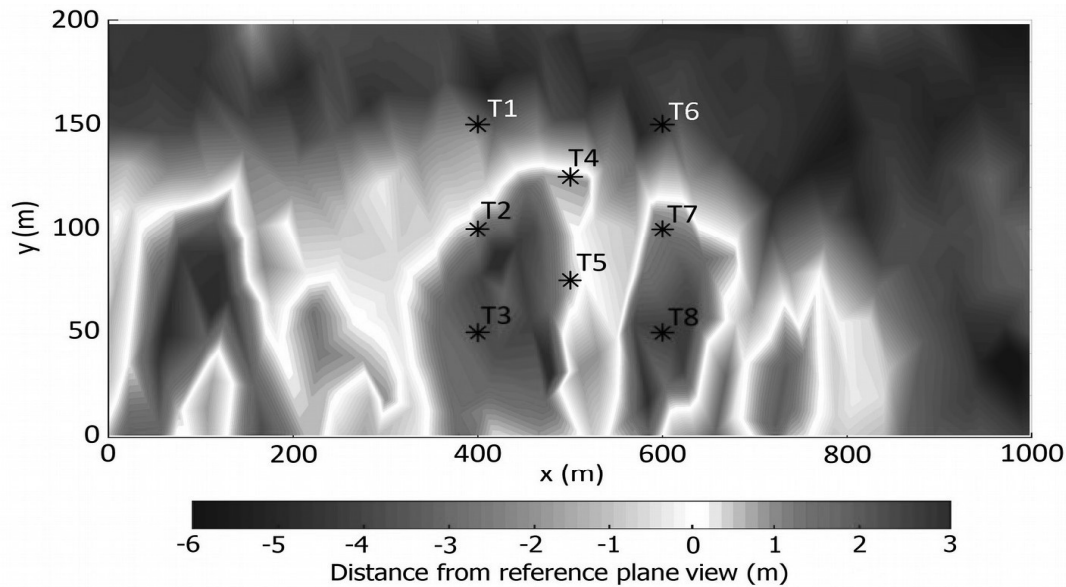
Figure 5 - Distance from the horizontal plane defined to plot synoptic views of numerical results with the locations of turbines in array configuration C1. Negative values indicate that the turbine was located below the horizontal plane view while positive values indicate that the turbine was located above this plane.

# 3. Results and discussion

## 3.1. Model validation

The evaluation of model predictions was performed against available in-situ observations of current magnitude and direction at point $p$, located in the north-eastern part of the Fromveur Strait (5.036°W; 48.449°N) (Figs. 3b and 6, Tab. 1). These observations were acquired by the French Navy SHOM ("Service Hydrographique et Océanographique de la Marine") with a RDI 600 kHz ADCP (Acoustic Doppler Current Profiler) between March 19th and April 2nd 1993. Measurements were provided, every 2 m, between 6 and 52 m above the seabed. The model simulated 13 days between March 17th and March 30th 1993 and the comparison between observations and predictions was conducted at 10 and 25 m above the bed. Particular interest was given to the 10 m level that corresponds to the operating height of horizontal-axis turbines within the Fromveur Strait [33].
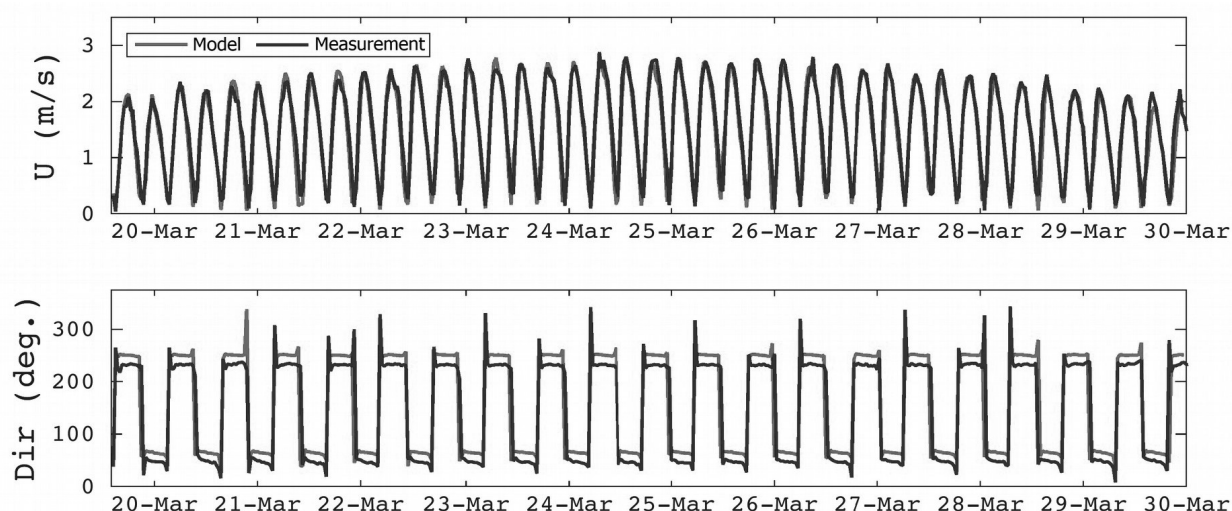
320

325

330

13

Figure 6 - Measured (blue line) and computed (red line) time series of the magnitude and direction (anticlockwise convention from the East) of the current, 10 m above the bed, at point p between 19th and 30th March 1993.

| Height above the bed (m) | $RE_{int}$ | $RE_{dir}$ | $MAE_{int}$ (m.s$^{-1}$) | $MAE_{dir}$ (deg.) |
|---|---|---|---|---|
| 10 | 0.98 | 0.95 | 0.13 | 20.2 |
| 25 | 0.98 | 0.94 | 0.13 | 20.2 |

Table 1 - Statistical parameters for the evaluation of the magnitude and direction of the current at 10 and 25 m above the bed. *RE* is the index of agreement and *MAE* is the mean average error.

An overall good agreement was obtained between the numerical model and the measurements of current magnitude, at 10 and 25 m above the bed, with indexes of agreement
335 *RE* of 0.98 (Tab. 1). Confirming the numerical investigations conducted by Guillou and Thiébot [13] and Guillou et al. [33], predictions reproduced the observed weak current asymmetry, characterised by slightly larger current magnitudes during south-western directed ebb than north-eastern directed flood (Fig. 6). Larger differences were obtained for the estimations of current direction, with mean averaged errors of 20.2° at both elevations above
340 the sea bed. However, these differences were found consistent with the numerical outputs established by Guillou and Thiébot [13] reproducing the abrupt changes between south-west and north-east directed velocities. Following the assessment of model's performance conducted by Guillou and Thiébot [13] within the Fromveur Strait, this local evaluation was supplemented by a synoptic comparison of ROMS predictions with numerical estimations
345 provided by the French Navy SHOM, during mean spring tidal conditions, at the scale of the Fromveur Strait [61]. Figure 7 shows the comparison of ellipses of depth-averaged tidal

14

currents predicted by our ROMS model and provided by the SHOM in mean spring tidal conditions. This spatial evaluation confirmed the ability of the numerical model to reproduce the temporal and spatial variabilities of currents, during mean spring tidal conditions, within
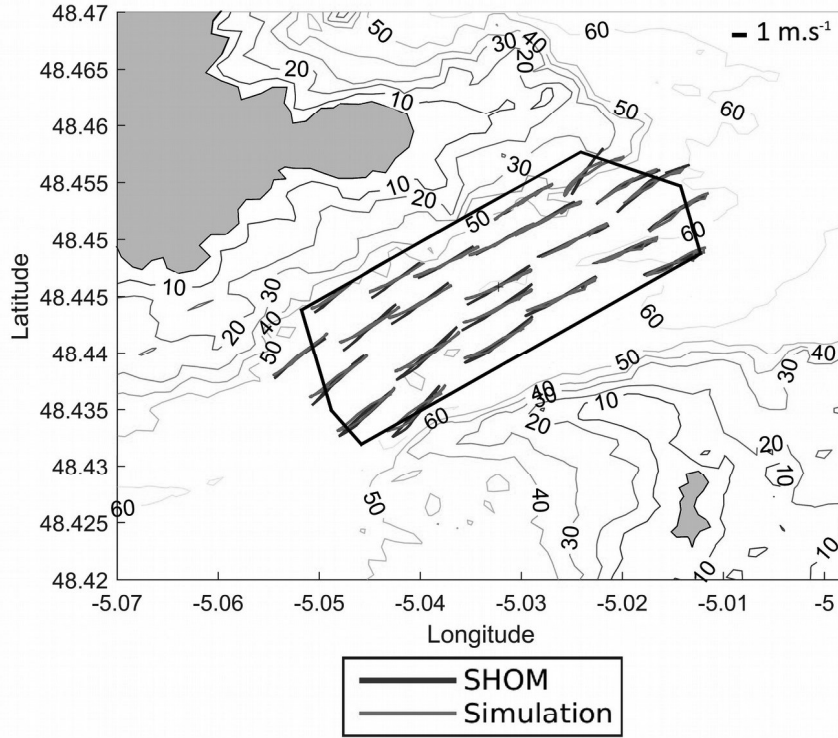
350 the tidal farm area.



Figure 7 - Current ellipses at 10 m above the bed (approximate hub height) for mean spring tidal conditions (blue) issued from the SHOM database [41] and (red) predicted by ROMS. Contours show bathymetry in metres relative to mean sea level.

## 3.2. Tidal asymmetry and directional misalignment

355

Fig. 8 shows the spatial distribution of the tidal energy resource metrics, $A_s$ and $\beta_s$, for asymmetries in current magnitude and direction, respectively, computed for mean spring tidal conditions, within the area of interest for turbine implementation. As exhibited by a series of numerical investigations [31,32], tidal straits are often characterised by prominent

360 asymmetries in current magnitude that can be described by the relative phase lag between the principal lunar semi-diurnal constituent $M_2$ and its first quarter-diurnal harmonic $M_4$. Confirming maps established by Guillou et al. [7] with high-resolution tidal harmonic database in western Brittany and the western English Channel, the spatial distribution of the metric $A_s$, within the Fromveur Strait, shows a central symmetrical area (small values of $A_s$)

365 that separates north-eastern and south-western asymmetrical regions (Fig. 8a). The asymmetry

15

in current magnitude was particularly pronounced in the north-eastern part of the domain, exhibiting a difference of 50% between peak ebb and peak flood. However, these differences reduced to less than 5% in the central area. As discussed by Thiébaut and Sentchev [62], Guillou and Thiébot [13], and Guillou and Chapalain [32], this spatial distribution is associated with a northern area experiencing northeast-directed flood-dominated flows, and a southern area experiencing southward ebb-dominated currents. Effectively, this means that the area identified for tidal energy extraction in the Fromveur Strait is a region of velocity divergence, and such regions have been shown to have reduced environmental impacts to sediment dynamics [63]. The generated practical power was estimated by Guillou et al. [7] at an asymmetrical location with $A_s$=0.12 from neap to spring conditions, revealing variations in energy extraction of over 60% between peak ebb and peak flood. The spatial distribution of the metric $\beta_s$ also exhibited spatial variations, with highest values in the south-western and northern extremities of the area of interest, mainly in the vicinity of shoals and the coastline (Fig. 8b). Such directional asymmetry was also identified by Lewis et al. [60] and Guillou et al. [7] in limited locations, seemingly associated with tidal recirculations appearing around headlands in shallow waters. However, the predicted values remained below 15° over the greatest part of the area of interest which accounts, from a simple relationship based on the cube of the cosine angle, to differences below 10% in energy extraction between peak ebb and peak flood. Whereas these two symmetrical areas may be targeted to deploy the turbine array, the asymmetry in current magnitude was found to result in stronger asymmetry in energy extraction than the asymmetry in current direction, within the Fromveur Strait. This confirms a series of numerical investigations conducted at a number of tidal stream energy sites [31,32, 64]. The symmetrical area in current magnitude was thus retained to position the array. Considering those results, the domain G3 was positioned within an area characterised by a current misalignment between peak ebb and peak flood of 13° in mean spring tidal conditions retaining the dimensions and the orientation (with respect to the longitude) described in section 2.3.
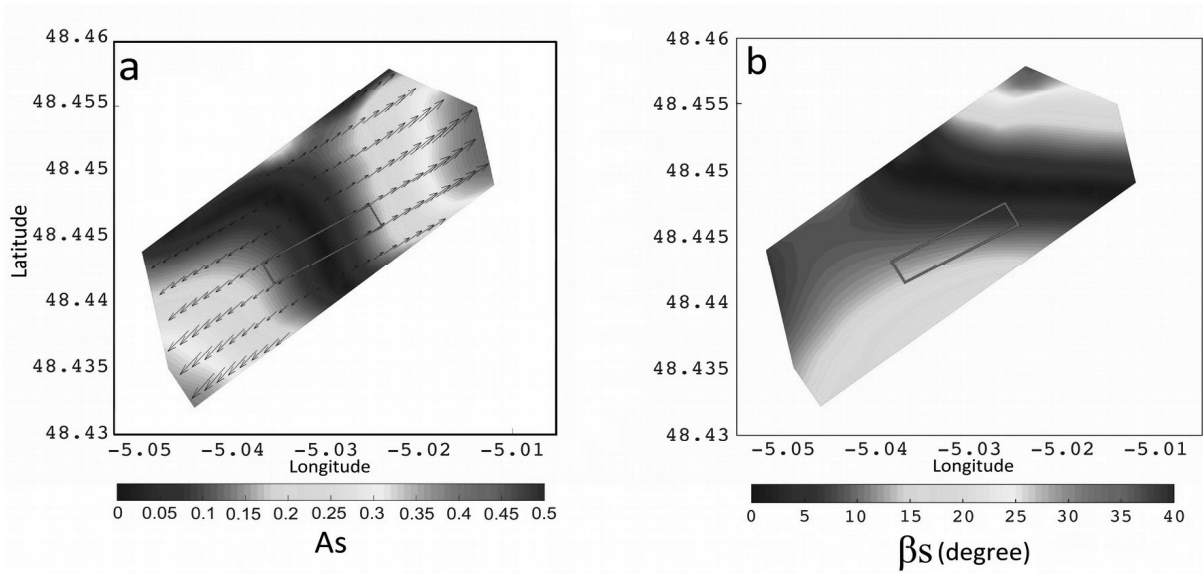
Figure 8 - Spatial distribution of parameters (a) $A_s$ and (b) $\beta_s$ in mean spring tidal conditions within the area of interest for the implementation of tidal stream devices. The red box delimits the innermost nested domain G3. The arrows in (a) show the residual tidal currents in mean spring tidal conditions.

## 3.3. Initial staggered array configuration C1

Fig. 9 shows the horizontal plane maps of flow velocity and turbulent kinetic energy at times of peak ebb and flood during a tidal cycle that is representative of mean spring tidal conditions, for the initial array layout C1. The orientation of the computational grid, described in Section 2.3, was aligned along the direction of the peak ebb current, for mean spring tide, within the Fromveur Strait. During peak ebb, the predicted spatial distribution of current velocity was thus found consistent with the wake-field study of Bai et al. [21] exhibiting, for a current aligned with turbines' axes, reduced interactions between wakes that develop into the devices' inter-space (Figs. 9a and b). However, slight interactions were found between wakes of the upstream line R3 and the downstream line R1. Wakes of line R3 overlapped thus wakes of line R1, resulting in enhanced turbulent kinetic energy in wakes of the downstream line (Fig. 9b). Nevertheless, there was minimal impact on energy extraction of the downstream line (R1), the distance of 20D between lines R1 and R3 being sufficient to recover more than 95% of the flow velocity. This resulted in a decrease below 10% of the mean power output (averaged per devices) for R1 in comparison with R3 (Tab. 2). This result was confirmed by comparing, for peak ebb conditions, the vertical profiles of current velocity at distances of 6, 12 and 18D downstream turbines T7 and T2 that were positioned at similar elevations above the seabed (Fig. 10). Note that, 18D downstream T7 corresponded to a location 2D upstream T2. The vertical profile of current velocity recovered almost completely 18D downstream T7

limiting the interaction with T2. Indeed, the high ambient turbulence intensity induced a faster recovery of T7 turbine wake as reported by Nguyen et al. [26]. However, during peak ebb, the averaged power extracted per turbine along line R2 was 3.5% higher than the averaged power in the upstream line (R3). As exhibited by Nguyen et al. [49,50], this difference may be associated with the slight increase of current magnitude within the bypass flow associated with devices upstream. Nevertheless, differences in energy extraction remained small during peak ebb, characterised by a tidal current orientated along the axes of the turbines.
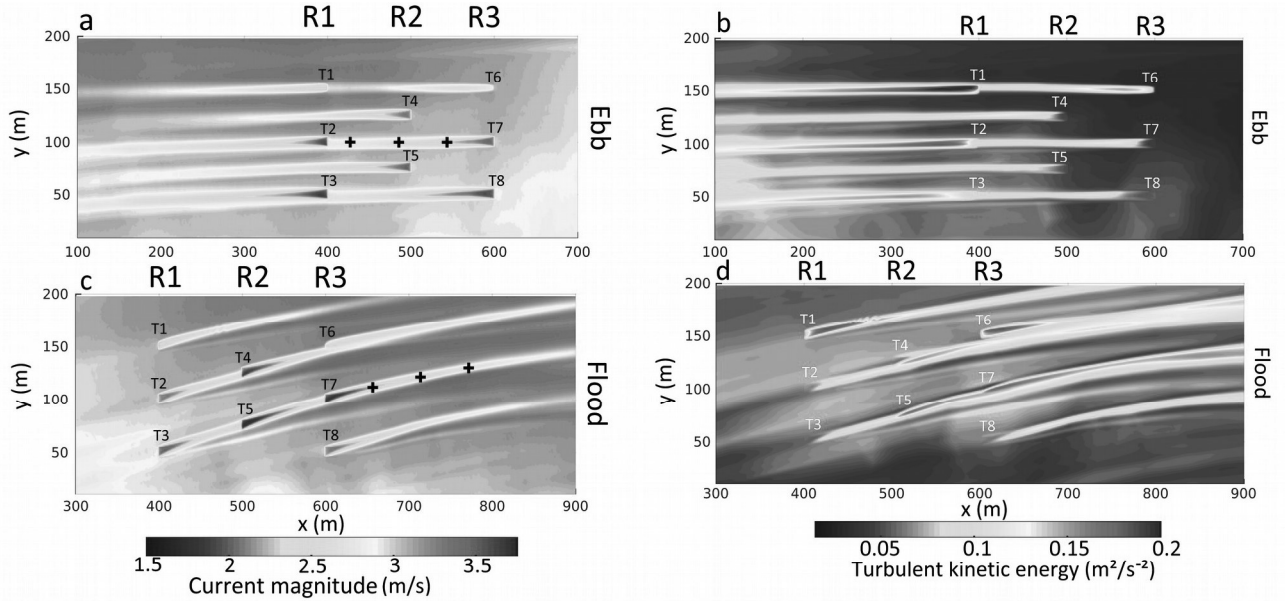


Figure 9 - Horizontal plane maps of (left) current magnitude and (right) turbulent kinetic energy at times of (a, b) peak ebb and (c, d) peak flood during a mean spring tide for array configuration C1. Black crosses show the position of points considered for the extraction of vertical velocity profiles in Fig. 11.

More significant changes occurred during peak flood, characterised by a tidal current deviation with a mean angle of 13° with respect to the (Ox) direction (Figs. 9c and d). This misalignment with respect to turbines' axes resulted in strong wake interactions that reduced the global array energy extraction by 15%, from 4.44 MW at peak ebb to 3.80 MW at peak flood, despite a 2 % difference in current speed between the flood and ebb. This highly imbalanced energy extraction resulted mainly from the overlapping of wakes between the two pairs of three turbines (i) T2, T4 and T6, and (ii) T3, T5 and T7. Nguyen et al. [49,50] defined this type of interaction as devices working in "tandem". This wake influence mainly impacted the energy extraction of the central row R2, with an average power per turbines estimated 23% lower than in the upstream row R1 (Tab. 2). The reduction in energy extraction for the downstream line R3 was less pronounced (-2%). Indeed, turbine T8 was located in the free stream (not impacted by upstream wakes) and exhibited the most important contribution to energy extraction across the array. The turbine T6 was furthermore located deeper than the

435 other devices (Fig. 5), which limited the influence of the upstream wake generated by turbine T4 on its energy extraction. Confirming the numerical investigation conducted by Lo Brutto et al. [65], a relative stabilisation of energy extraction was furthermore obtained for downstream devices working in "tandem". At peak flood, the power output of downstream turbines T5 and T7 was thus estimated around 0.40 MW, while it reached 0.52 MW for upstream turbine T3.

440 This evolution in energy extraction may be attributed to the increase in the turbulent kinetic energy, up to $0.15 \, \mathrm{m^2.s^{-2}}$, along the wake of the middle turbine T5 which induced a rapid recovery of the velocity magnitude and restricted the reduction in power output from turbine T7 [66,27,30]. However, despite this influence of the increased turbulence intensity, T7 wake recovered over a longer distance at peak flood than at peak ebb (Fig. 9). This wake asymmetry

445 was confirmed by comparing the vertical profiles of velocity magnitudes 6D, 12D and 18D downstream of turbine T7 at times of peak ebb and flood (Fig. 11). Indeed, due to wake overlap, the velocity deficit downstream of T7 was higher at peak flood, while it was not influenced by the other turbines at peak ebb, and recovered almost completely 18D downstream of the turbine.

450 It should finally be noted that the misalignment in current direction at peak flood resulted in a slight increase of the current magnitude along the southern part of the turbine wakes (Fig. 9c), reaching a maximum of 6% (compared to a simulation without turbines) at 15D downstream. However, as numerical investigations with the AD method relied mainly on a tidal current along the axis of the turbines, this acceleration zone has not, to our knowledge, been reported

455 elsewhere. Roc et al. [23] examined the application of the AD in ROMS to simulate the effects of a turbine array on tidal hydrodynamic conditions in front of a symmetrical headland characterised by oblique currents. However, this modelling study compared the estimation of the power captured by the farm with different methods, setting aside a refined estimate of the velocity profile along the wake of devices. Whereas extensive investigations would be

460 required to fully test the robustness of the method, the numerical results obtained with our AD implementation in ROMS illustrated its ability to adapt the array layout to the tidal hydrodynamic conditions of a realistic stream energy site.
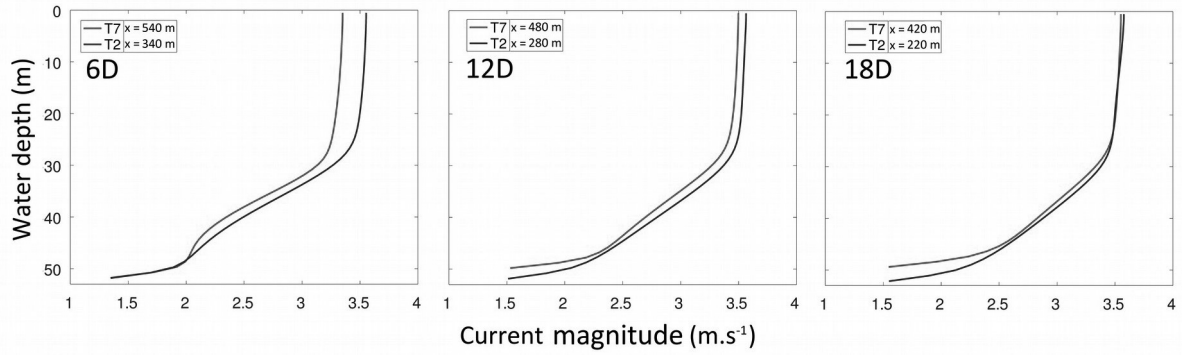
Figure 10 - Vertical profiles of current magnitude 6 (a), 12 (b) and 18D (c) downstream turbines T7 and T2 at peak ebb in configuration C1. The profiles on every sub-figures are thus provided at different locations within the array but corresponds to similar locations upstream devices. The indicated x-distance is in relation to Fig. 9.
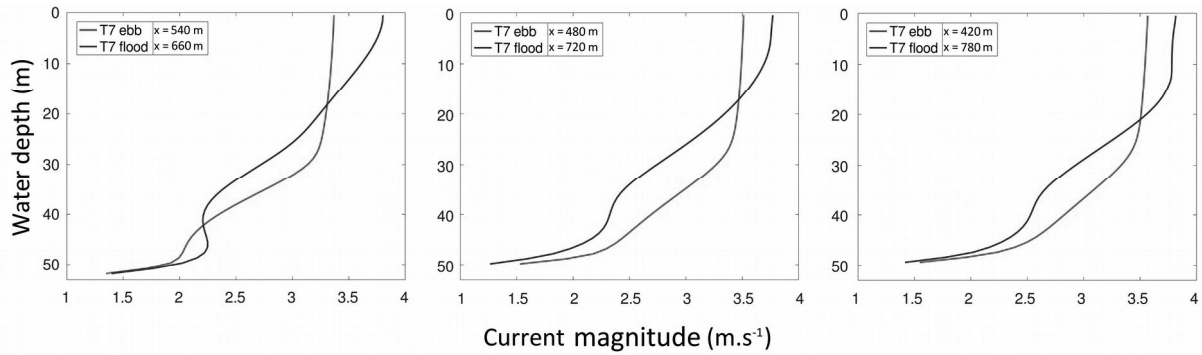


Figure 11 - Vertical profiles of current magnitude at a distance (a) 6D, (b) 12D, and (c) 18D downstream of turbines T7 at times of peak ebb and flood for configuration C1. The locations of the profiles are provided on Figs. 9 a and c. The indicated x-distance is in relation to Fig. 9.

### 3.4. Adapted staggered array configuration C2

Based on the previous predictions in terms of wake interactions and power output, the array layout was adapted to peak flood current in an attempt to maximise energy extraction. A simple trigonometric estimation, based on an incidence angle of 13°, demonstrated that a lateral spacing of 3D should avoid the overlapping of turbine wakes at peak flood. Configuration C2 was thus adapted from C1 by reducing the lateral spacing from 5D to 3D, while maintaining the longitudinal spacing of 10D (Fig. 4). Fig. 12 shows horizontal plane maps of flow velocity and turbulent kinetic energy at times of peak ebb and peak flood for a mean spring tide with this new array layout C2.
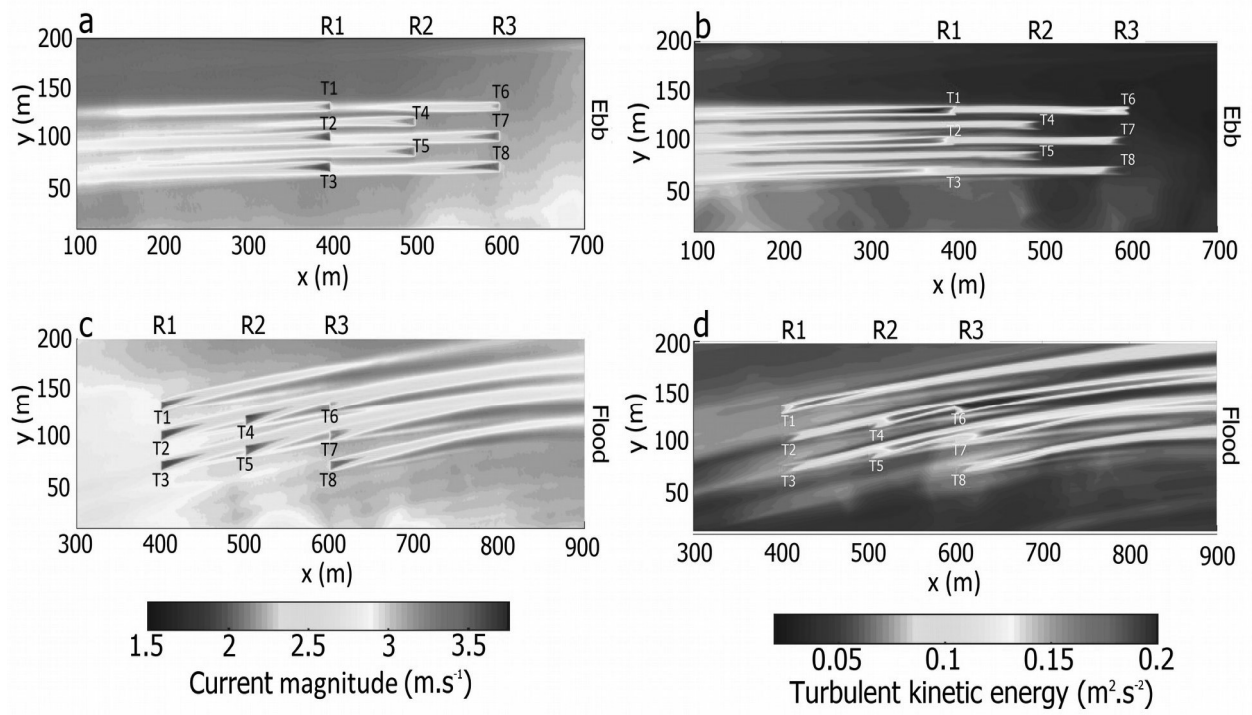
Figure 12 – Horizontal plane maps of (left) current magnitude and (right) turbulent kinetic energy at times of (a,b) peak ebb and (c,d) peak flood of a mean spring tide for the array configuration C2.

475      As expected, reduced differences were obtained at peak ebb between the two configurations C1 and C2 (Figs. 9a,b and 12a,b). The current velocity, turbulent kinetic energy and power output were thus characterised by similar values as in the previous layout, with a slight increase of eneryg extraction in row R3 (0.61 MW compared to 0.57 MW in C1 configuration, Tab. 3), seemingly associated with the different locations of turbines T6 and T8 480   within the tidal current flow.

     However, wake overlaps were significantly reduced at peak flood (Figs. 12c and d). While the upstream line was weakly affected, resulting in nearly the same power outputs between C1 and C2, increased differences were obtained for the downstream lines R2 and R3 (Tab. 3). The energy extraction averaged per devices for rows R2 and R3 increased by 35 and 30%, 485   respectively. For devices T3, T5 and T7 previously working closely in "tandem", the energy extraction of the downstream turbines increased by nearly 30% between configurations C1 and C2. Indeed, in the new configuration C2, the downstream devices were no longer positioned in the wakes of upstream turbines, and were even positioned in the acceleration area reported along the wakes of devices (Section 3.3). Further, the turbulent kinetic energy 490   increased for the downstream devices, which led to a rapid recovery of velocity magnitude within the wakes. This effect could be explained by the mixing between the high velocity present in the bypass flow and the lower velocity in the inner wake region. According to Ahmadi [67], the increased turbulence intensity downstream the turbine induced that the

21

radial momentum transport between the bypass flow and the inner wake region started closer to the turbine thus increasing the recovery. However, this increased turbulence may also induce an important increase in fatigue loadings. In the experimental study conducted by Blackmore et al. [68], the fluctuation of load with low turbulence intensity was thus estimated between 5 and 10% of the mean value (averaged among the different tests). These fluctuations in mean load rose to 30-45% with higher turbulence intensity thus affecting the downstream turbines durability. Moreover, this increased recovery may also be exacerbated by the variation of the initial turbulent kinetic energy and current magnitude found in the new locations but it only contributes to less than 1% of the increase of energy extraction.

The increase in power output at peak flood balanced the energy extraction of the array during the mean spring tidal cycle. The global array energy extraction was thus estimated at 4.53 MW at peak ebb (against 4.44 MW in configuration C1) and 4.47 MW at peak flood (against 3.80 MW in C1) with a difference of only 2% (compared to a difference of 15% between peak ebb and peak flood for C1). Moreover, this new configuration does not further alter the flow field, because the average change between C1 and C2 in term of velocity deficit and turbulence was estimated to be lower than 1% over the entire domain. In mean spring tidal conditions, configuration C2 was thus more appropriate than configuration C1 as it maximises the power output and balanced energy extraction between ebb and flood without inducing a higher environmental impact. These aspects are significant for tidal stream energy extraction within the Fromveur Strait, since they reduce the temporal variability of electricity generated and facilitating its integration into the power grid of the island of Ushant as a substitute to the diesel generators currently used.

| Array layout | R1 (MW) | R2 (MW) | R3 (MW) | Total (MW) |
|:---:|:---:|:---:|:---:|:---:|
| C1 | 0.51 | 0.39 | 0.50 | 3.80 |
| C2 | 0.52 | 0.54 | 0.61 | 4.47 |

Table 3 - Power output averaged per devices for rows R1, R2 and R3 and total power output in configurations C1 and C2 at peak flood of a mean spring tide.

# 4. Conclusion

A modified version of the three-dimensional ROMS model, which integrates an Actuator Disk (AD) sub-model, was implemented at a tidal stream energy site in the Fromveur Strait to investigate the interactions of turbine wakes in two array configurations designed to fulfil a

22

significant part of the electricity demand of the isle of Ushant. Two configurations of eight turbines with a diameter of 10 m were considered, in mean spring tidal conditions, with varying lateral spacing between devices from a layout recommended in the scientific literature to an adapted configuration. Numerical simulations of the undisturbed flow field were assessed against ADCP observations within the area of interest, and using an available current database. The main outcomes of the study are as follows:

1. Two tidal energy metrics were considered to describe the asymmetries in tidal current magnitude and direction within the area targetted for the installation of an array of turbines. Predictions revealed contrasting spatial distributions. In agreement with previous studies, the region with equivalent magnitude of peak ebb and flood was identified in the centre of the Fromveur Strait, whereas the region with reduced misalignment was located further north. However, the asymmetry in current magnitude was found to result in stronger variability in power output than the asymmetry in current direction. The area with reduced asymmetry in current magnitude was thus used to implement the turbine array.

2. The area covered by the tidal farm was characterised by a misalignment in current direction between peak ebb and peak flood, estimated at 13° during mean spring tidal conditions. Turbine axes were positioned along the peak ebb current direction. This resulted in asymmetrical wake shapes between ebb and flood which increased, for the recommended staggered array layout, the variability in energy extraction during a mean spring tidal cycle. The array output resulted in a difference of 15% between peak ebb and peak flood.

3. The array configuration was adapted to the tidal current conditions within the Fromveur Strait by reducing the (centre to centre) lateral spacing from 5D to 3D. Whereas reduced differences were obtained at peak ebb when currents were aligned with the turbine axes, more significant effects were predicted at peak flood, characterised by a current deviation with respect to the turbine axes. The reduction in lateral spacing was found to reduce the effect of wake overlap, and enhance the generation of turbulent kinetic energy, improving the velocity recovery downstream. This resulted in differences below 2% between the power extracted at peak ebb and peak flood during mean spring tidal conditions. However, this enhanced generation of turbulent kinetic energy at peak flood could also affect the downstream turbines durability and should thus be investigated in further studies.

4. An acceleration zone was found along the southern part of deviated wakes at peak flood, and may be attributed to the implementation of the AD method in misalignment tidal current

conditions. However, further numerical studies are required to confirm the spatial distribution of turbine wakes.

555    The findings from these numerical simulations provide potential developers with more information about turbine array layouts in a tidal stream energy site characterised by spatially-varying water depth, bottom roughness and time-evolving tidal conditions. However, several simplifications were considered. The contributions of wind and waves were thus neglected. Those two factors could modify the current magnitude and direction and so affect the array

560    production difference between peak ebb and peak flood within the study area. Waves may thus impact the tidal circulation and associated kinetic energy by (1) increasing the apparent bottom friction felt by currents above the wave boundary layer (non-linear interactions of wave and current bottom boundary layers) and (2) generating wave-driven currents in regions of wave breaking. In the Fromveur Strait, these effects were quantified by Guillou et al. [33]

565    exhibiting a reduction of 12% of the available mean spring tidal stream potential during extreme wave conditions. However, in the present investigation, these modulations were disregarded focusing on turbines' wakes interactions in tide-dominated conditions as these conditions prevail in the site of application. Before considering these processes in numerical simulations of turbine wake interactions, further investigations must be conducted to extend

570    the number of tested tidal hydrodynamic conditions and array configurations. These simulations were thus restricted to mean spring tidal conditions, and extended tidal hydrodynamic conditions such as exceptional spring tides or neap tides may be investigated to assess changes induced on turbine wake interactions within the array. Moreover, this study was restricted to only two array configurations, and the influence of longitudinal and lateral

575    spacings, as well as varying thrust coefficients, may be explored. In this study, the AD method was assessed against experimental flume observations. Whereas numerical studies were conducted to evaluate the scale applicability of this method within the Fromveur Strait, further comparisons with in-situ observations (when available) in the wake of the Sabella D10 turbine deployed within this environment would confirm the reliability of the AD method.

580    Nevertheless, this study provided some early information about the influence of the tidal asymmetry and misalignment on an array, and may be considered as a first step to adapt the layout to asymmetrical currents in order to maximise power output.

# Acknowledgments

# References

[1] Fraenkel PL., Marine current turbines: pioneering the development of marine kinetic energy converters, Proceedings of the Institution of Mechanical Engineers Part A Journal of Power and Energy 221 (2007) 159-69.

[2] Khan M.J., Bhuyan G., Iqbal M.T., Quaicoe J.E., Hydrokinetic energy conversion systems and assessment of horizontal and vertical axis turbines for river and tidal applications: A technology status review, Applied Energy 86 (2009) 1823-1835.

[3] Allo JC, Dhomé D, Battaglia B, Feedbacks from Sabella D10 1 MW sea trials (2016).

[4] Robins P.E., Neill SP.P, Lewis M.J., Ward S., Characterising the spatial and temporal variability of the tidal-stream energy resource over the northwest European shelf seas, Apply Energy 147 (2015) 510-522.

[5] Neill S.P., Hashemi M.R., Lewis M.J., Tidal energy leasing and tidal phasing, Renewable Energy 85 (2016) 580-587.

[6] Coles D.S., Blunden L.S., Bahaj A.S., Assessment of the energy extraction potential at tidal sites around the Channel Islands, Energy 124 (2017) 171-186.

[7] Guillou N., Neill S.P., Robins P.E., Characterising the tidal stream power resource around France using a high-resolution harmonic database, Renewable Energy 123 (2018) 706-718.

[8] Defne Z., Hass K.A., Fritz H.M., Numerical modelling of tidal currents and the effects of power extraction on estuarine hydrodynamics along the Georgia coast, USA, Renewable Energy, 36 (2011) 3461-3471.

[9] Ashall L.M., Mulligan R.P., Law B.A., Variability in suspended sediment concentration in the Minas Basin, Bay of Fundy, and implications for changes due to tidal power extraction, Coastal Engineering, 107 (2016) 102-115.

[10] Waldman S., Yamaguchi S., Murray R.O., Woolf D., Tidal resource and interactions between multiple channels inthe Goto Islands, Japan, International Journal of Marine Energy, 19 (2017) 332-344.

[11] Marta-Almeida M., Cirano M., Guedes Soares C., Lessa G.C., A numerical tidal stream energy assessment study for Baia de Todos os Santos, Brazil, Renewable Energy, 107 (2017) 271-287.

[12] Thiébot J., Bailly du Bois P., Guillou S., Numerical modelling of the effect of tidal stream turbines on the hydrodynamics and the sediment transport – Application to the Alderney Race (Raz Blanchard) France, Renewable Energy 75 (2015) 356-365.

[13] Guillou N., Thiébot J., The impact of seabed rock roughness on tidal stream power extraction, Energy 112 (2016) 762-773.

[14] Sørensen J., Shen W.(2002),Numerical modeling of wind turbine wakes, Journal of Fluids Engineering,124,393-399.

[15] Baba-Ahmadi M.H., Dong P.(2017),Numerical simulations of wake characteristics of a horizontal axis tidal stream turbine using actuator line model, Renewable Energy,113,669-678.

[16] Baratchi F., Jeans T.L., Gerber A.G.(2017),Actuator line simulation of a tidal turbine in straight and yawed flows, International Journal of Marine Energy,19,235-255.

[17] Liu C., Hu C.(2019),An actuator line - immersed boundary method for simulation of multiple tidal turbines, Renewable Energy,136,473-490.

[18] Frost C., Morris C.E., Mason-Jones A., O'Doherty D.M., O'Doherty T.,The effect of tidal flow directionality on tidal turbine performance characteristics, Renewable Energy, 78 (2015) 609-620.

[19] Park Se., Park Su., Rhee S.H.,Influence of blade deformation and yawed inflow on performance of a horizontal axis tidal stream turbine, Renewable Energy, 92 (2016) 321-332.

[20] Frost C.H., Evans P.S., Harrold M.J., Mason-Jones A., O'Doherty T., O'Doherty D.M., The impact of axial flow misalignment on a tidal turbine, Renewable Energy, 113, (2017) 1333-1344.

[21] Bai L., Spence R.R.G., Dudziak G., Investigation of the influence of array arrangement and spacing on Tidal Energy Converter (TEC) performance using a 3-dimensional CFD

model, In Proceedings of the 8th European Wave and Tidal Energy Conference, Uppsala, Sweden (2009) 654-660.

[22] Harrison M.E., Batten W.M.J., Myers L.E., Bahaj A.S., Comparison between CFD simulations and experiments for predicting the far wake of horizontal axis tidal turbines, In IET Renewable Power Generation (2010).

[23] Roc T., Greaves D., Thyng K.M., Conley D.C., Tidal turbine representation in an ocean circulation model : Towards realistic application, Ocean engineering 78 (2014) 95-111.

[24] Liu J., Lin H., Purimitla S.R., Wake field studies of tidal current turbines with different numerical methods, Ocean Engineering, 117 (2016), 383-397.

[25] Shives M., Crawford C., Tuned actuator disk approach for predicting tidal turbine performance with wake interaction, Internation Journal of Marine Energy, 17 (2017), 1-20.

[26] Mycek P., Gaurier B., Germain G., Pinon G., Rivoalen E., Experimental study of the turbulence intensity effects on marine current turbines behaviour. Part I : One single turbine, Renewable Energy, 66 (2014a), 729-746.

[27] Mycek P., Gaurier B., Germain G., Pinon G., Rivoalen E., Experimental study of the turbulence intensity effects on marine current turbines behaviour. Part II: Two interacting turbines, Renewable Energy, 68 (2014b), 876-892.

[28] Goward-Brown A.J., Neill S.P., Lewis M.J., Tidal energy extraction in three-dimensional ocean models, Renewable Energy 114 (2017) 1-17.

[29] Bai G., Li J., Fan P., Li G., Numerical investigation of the effects of different arrays on power extractions of horizontal axis tidal current turbines, Renewable Energy 53 (2013) 180-186.

[30] Nguyen V.T., Guillou S., Thiébot J., Santa Cruz A., Modelling turbulence with an Actuator Disc representing a tidal turbine, Renewable Energy, 97 (2016) 625-635.

[31] Neill P.S., Hashemi R.M., Lewis J.M., The role of tidal asymmetry in characterizing the tidal energy resource of Orkney, Renewable Energy 68 (2014) 337-350.

[32] Guillou, N. and Chapalain, G., Tidal Turbines' Layout in a Stream with Asymmetry and Misalignment, Energies 10 (2017) 1892.

[33] Guillou, N., Chapalain, G., Neill, S.P., The influence of waves on the tidal kinetic energy resource at a tidal stream energy site, Applied Energy 180 (2016) 402-415.

[34] Guillou, N. and Thiébot, J., Impact environnemental d'un parc hydrolien: sensibilité des prédictions à la rugosité de fond, 15èmes Journées de l'Hydrodynamique, Brest (2016).

[35] Guillou, N. and Chapalain, G., Assessing the impact of tidal stream energy extraction on the Lagrangian circulation, Applied Energy 203 (2017) 321-332.

[36] Guillou, N. and G. Chapalain, Evaluating the Effects of Tidal Turbines on Water-Mass Transport with the Lagrangian Barycentric Method, In Sixth International Conference on Estuaries and Coasts (ICEC) (2018).

[37] Shchepetkin A.F., McWilliams J.C., The regional oceanic modelling system (ROMS) : a split-explicit, free-surface, topography-following-coordinate oceanic model, Ocean Modelling 9 (2005) 347-404.

[38] Smagorinsky J., General circulation experiments with the primitive equations, Monthly weather review 91(3) (1963) 99-164.

[39] Umlauf L., Burchard H., Island wakes in shallow coastal water, Journal of Geophysical research atmospheres 61 (2003) 235-265.

[40] Killworth P.D., Stainforth D., Webb D.J., Paterson, The development of a free-surface Bryan-Cox-Semtner ocean model, J. Phys. Ocean.,, 21 (1991), 1333-1348.

[41] Haidvogel, D. B., H. G. Arango, K. Hedstrom, A. Beckmann, P. Malanotte-Rizzoli, and A. F. Shchepetkin, Model evaluation experiments in the North Atlantic Basin : Simulations in nonlinear terrain-following coordinates, Dyn. Atmos. Oceans 32 (2000) 239-281.

[42] Betz A., Das maximum der theoretisch moglichen ausnutzung des windes durch windmotoren, Gesamte Turbinenwesen Heft 26 (1920).

[43] Hunter W., Nishino T., Willden R.H.J, Investigation of Tidal Turbine using 3D Reynold-Averaged Navier-Stokes Simulations, International Journal of Marine Energy 10 (2015) 39-51.

[44] Thiébot J., Guillou S., Nguyen V.T., Modelling the effect of large arrays of tidal turbines with depth-averaged Actuator Disk, Ocean Engineering 126 (2016) 267-275.

[45] Myers L., Bahaj A.S., Simulated electrical power potential harnessed by marine current turbine arrays in the Alderney Race, Renewable Energy 30 (2005) 1713-1731.

[46] Hansen M.O.L., Aerodynamics of Wind Turbines, London Sterling, VA 28 (2008).

[47] Roc T., Conley D.C., Greaves D., Methodology for tidal turbine representation in ocean circulation model, Renewable Energy 51 (2013) 448-464.

[48] Myers L.E., Bahaj A.S., Experiment analysis of the flow field around horizontal axis tidal turbines by use of scale mesh disk rotor simulators, Ocean Engineering 37 (2010) 218-227.

[49] Nguyen V.T., Guillou S., Santa Cruz A., Shielkh Elsouk M.N., Thiébot J., Effect of the current direction on the energy production of a tidal farm, In Proceedings of the 12th European Wave and Tidal Energy Conference, Cork Ireland (2017).

[50] Nguyen V.T., Santa Cruz A., Guillou S., Shiekh Elsouk M.N., Thiebot J., Effects of the current direction on the energy production of a tidal farm : The case of Raz Blanchard (France), ,Energies,12,2478 (2019).

[51] Funke S.W., Kramer S.C., Piggott M.D., Design optimisation and resource assessment for tidal-stream renewable energy farms using a new continuous turbine approach, Renewable Energy 99 (2016) 1046-1061.

[52] Loubrieu B., Bourillet J., Moussat E., Bathy-morphologique régionale du Golfe de Gascogne et de la Manche, modèle numérique, Tech. rep., Ifremer (2008).

[53] Louvart L., Grateau C., The Litto3D project, Oceans 2005-Europe, Brest : France (2005). http://professionnels.ign.fr/litto3d

[54] Hamdi A., Vasquez M., Populus J. ,Cartographie des habitats physiques EUNIS – côte de France, Technical report (2010). dyneco/ag/10-26/jp.

[55] Egbert G., Bennett A., Foreman M., Topex/Poseidon tides estimated using a global inverse model, Journal of Geophysical Research 99 (1994) 24821-24852.

[56] Flather R.A., A tidal model of the northwest european continental shelf, Mémoire de la Société Royale des Sciences de Lièges 6 (1976) 141-164.

[57] Chapman D.C., Numerical treatment of cross-shelf boundaries in a barotropic coastal ocean model, Journal of Physical Oceanography 15 (1985) 1060-1075.

[58] Orlanski I., A simple boundary condition for unbounded hyperbolic flows, Journal of Computational Physics 21(3) (1976) 251-269.

[59] Willmot C., On the validation of models, Physical Geography 2 (1981) 184-194.

[60] M. Lewis, S. Neill, P. Robins, M. Hashemi, Resource assessment for future generations of tidal-stream energy arrays, Energy 83 (2015) 403-415.

[61] SHOM (2015). https://data.shom.fr/ (accessed in 2015).

[62] Thiébaut M., Sentchev A., Assymetry of tidal currents off the W.Brittany coast and assessment of tidal energy ressource around the Ushant Island, Renewable Energy 105 (2017) 735-747.

[63] Neill S.P., Litt E.J., Couch S.J., Davies, A.G., The impact of tidal stream turbines on large-scale sediment dynamics, Renewable Energy 34 (2009) 2803-2812.

[64] Piano M., Neill S.P., Lewis M.J., Robins P.E., Hashemi M.R., Davies A.G., Ward S.L., Roberts M.J., Tidal stream ressource assessment uncertainty due to flow asymmetry and turbine yaw misalignment, Renewable Energy 114 (2017) 1363-1375.

[65] Lo Brutto O.A., Nguyen V.T., Guillou S.S., Thiébot J., Gualous H., Tidal farm analysis using an analytical model for the flow velocity prediction in the wake of a tidal turbine with small diameter to depth ratio, Renewable Energy 99 (2016) 347-359.

[66] Blackmore T., Batten W.M.J., Bahaj A.S., Influence of turbulence on the wake of a marine current turbine simulator, Proceedings of the Royal Society vol. 470, issue 2170 (2014).

[67] Ahmadi M.H.B., Influence of upstream turbulence on the wake characteristics of a tidal stream turbine, Renewable Energy, 132 (2019), 989-997.

[68] Blackmore T., Myers L.E., Bahaj A.S., Effects of turbulence on tidal turbines : Implications to performance, blade loads, and condition monitoring, International Journal of Marine Energy, 14 (2016), 1-26.